

ORIGINAL RESEARCH

Targeted Intestinal Tight Junction Hyperpermeability Alters the Microbiome, Behavior, and Visceromotor Responses

Orsolya Incze^{1,2,*}, Valérie Bacquié^{1,*}, Maïwenn Olier-Pierre¹, Marion Rincel³, Belinda Ringot-Destrez⁴, Sandrine Ellero-Simatos¹, Hélène Eutamène¹, Colette Bétoulières¹, Julie Thomas³, Justin Laine³, Louise Gros³, Mathilde Lévêque¹, Renaud Leonard⁴, Cherryl Harkat¹, Catherine Robbe-Masselot⁴, Richard Roka², Muriel Mercier-Bonin¹, Vassilia Theodorou¹, Muriel Darnaudéry³, Jerrold R. Turner⁵, and Laurent Ferrier¹

¹UMR 1331 ToxAlim, French National Institute for Agriculture, Food, and Environment, Toulouse, France; ²First Department of Medicine, University of Szeged, Szeged, Hungary; ³UMR 1286, Nutrition and Integrative Neurobiology, University of Bordeaux, French National Institute for Agriculture, Food, and Environment, Bordeaux, France; ⁴Unité de Glycobiologie Structurale et Fonctionnelle, Université de Lille, Villeneuve d'Ascq, France; and ⁵Laboratory of Mucosal Barrier Pathobiology, Department of Pathology, Brigham and Women's Hospital, Harvard Medical School, Boston, Massachusetts

Markedly increased intestinal permeability occurs in inflammatory bowel disease, graft-versus-host disease, celiac disease, and multiple organ dysfunction. In these diseases, effectors of increased permeability include immune signaling,¹ microbiome,² and corticosteroids³ that, in part, signal through epithelial myosin light chain kinase (MLCK). More modest permeability increases occur in other disorders, including irritable bowel syndrome (IBS), autism spectrum disorder, depression, and stress-related disorders. However, data directly linking barrier loss to disease phenotypes are lacking.

To define the impact of modestly increased intestinal permeability, we studied transgenic mice with intestinal epithelial-specific constitutively-active myosin light chain kinase (CAMLCK) expression. This MLCK-dependent tight junction regulation increased intestinal permeability (Supplementary Figure S1A and B).¹ Nevertheless, postnatal growth (Supplementary Figure S1C), reproduction, intestinal transit (Supplementary Figure S1D) and intestinal histology, epithelial proliferation (a sensitive indicator of epithelial damage), and epithelial turnover are unaffected in CAMLCK transgenic (*CAMLCK^{Tg}*) mice.¹ In contrast, mucosal tumor necrosis factor- α , interferon- γ , interleukin (IL)-10, and IL-13 transcripts as well as numbers of lamina propria neutrophils, CD4⁺ T cells, and IgA⁺ plasma cells are modestly increased by CAMLCK expression.^{1,2} Subclinical inflammation is, therefore, present and, by microbiome-dependent, IL-17-mediated processes, affords partial protection from acute pathogen invasion.² Immune activation is nevertheless unlikely to amplify CAMLCK-driven permeability increases, as barrier function and ZO-1 anchoring are both acutely normalized by enzymatic MLCK inhibition.^{1,4}

We initially analyzed the gut microbiome of 31 wild-type (WT) and *CAMLCK^{Tg}* pups born to 8 WT dams. The microbiomes segregated by pup genotype but not dam (Supplementary Figure S1E) and included increased *Clostridium* and decreased Bacteroidetes, *Enterococcus spp.*, and *Prevotella* in *CAMLCK^{Tg}* mice (Supplementary Figure S1F).

Increased intestinal permeability can therefore cause dysbiosis-like microbiome shifts. Interestingly, maternal separation, which increases intestinal permeability, causes similar alterations and can be partially corrected by MLCK inhibitor-induced barrier restoration.⁵

Microbiome alterations overlapping with the above have been reported in IBS and autism spectrum disorder. We therefore asked if *CAMLCK^{Tg}* mice displayed anxiety-like behavior, as occurs in those disorders, using the open field test (Figure 1A). Both the percentage of distance traveled in the center and the fraction of time spent in the center of the open field were reduced in *CAMLCK^{Tg}* mice (Figure 1A); this did not reflect reduced locomotor activity, as total distance traveled in the entire area was similar in *CAMLCK^{Tg}* and WT mice (Figure 1A). These data are consistent with increased anxiety-like behavior in *CAMLCK^{Tg}* mice. Although the results cannot differentiate between direct effects of increased permeability and those requiring intermediate mediators, these data demonstrate that intestinal permeability increases can influence behavior.

Stress and increased permeability have been associated with enhanced visceral sensitivity in humans and rodents. Surprisingly, *CAMLCK^{Tg}* mice displayed striking visceral analgesia to colorectal distension relative to WT littermates (Figure 1B). Sensitivity was restored by enzymatic MLCK inhibition, water avoidance stress, or naloxone-mediated opioid receptor antagonism (Figure 1B). Although this effect of increased permeability on visceral sensitivity was unexpected, it is remarkably similar to the naloxone-reversible visceral analgesia reported in chronically stressed female rats⁶ and naloxone-sensitive inhibition of

*Authors share co-first authorship.

© 2020 The Authors. Published by Elsevier Inc. on behalf of the AGA Institute. This is an open access article under the CC BY-NC-ND license (<http://creativecommons.org/licenses/by-nc-nd/4.0/>).

2352-345X

<https://doi.org/10.1016/j.jcmgh.2020.02.008>

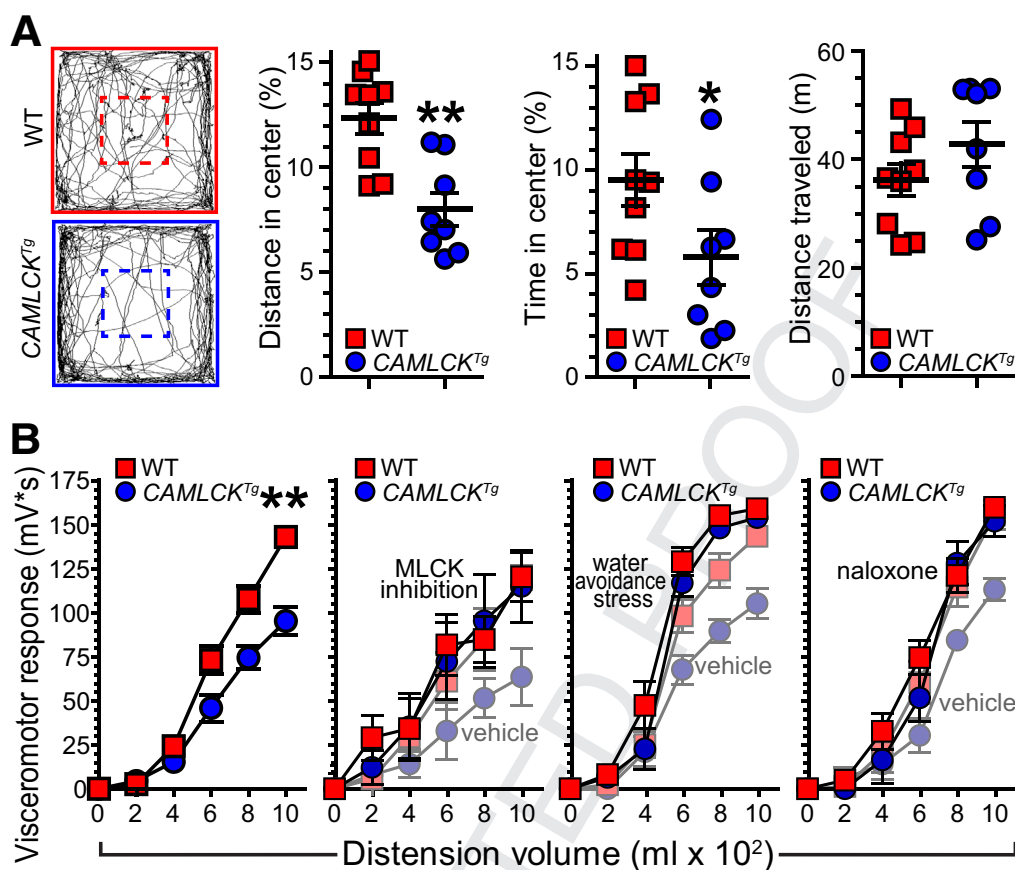


Figure 1. Increased intestinal permeability modifies behavior and visceral sensitivity. (A) Videotracking paths of representative WT and *CAMLCK^{Tg}* mice in the open field test. Percent distance traveled in the center (dashed lines), percent time in the center, and overall distance traveled in the entire field are shown. *CAMLCK^{Tg}* (blue circles, $n = 8$) and WT (red squares, $n = 9$) littermates were tested. Values are mean \pm SEM. * $P < .05$; ** $P < .01$, Mann-Whitney U test. (B) Stepwise colorectal distension-induced visceromotor responses in *CAMLCK^{Tg}* (blue circles, $n = 7$) were reduced relative to WT (red squares, $n = 7$) littermates. Genotype-specific differences were eliminated by MLCK inhibition, water avoidance stress, or naloxone treatment. $n = 5$ – 9 per condition; for each treatment (vehicle control *CAMLCK^{Tg}* and WT mice from the same experiment are shown with pale symbols in the last three graphs). Values are mean \pm SEM. **, $P < .01$, 2-way analysis of variance.

nociceptive neurons by supernatants of colitic human and murine tissues.⁷

Studies of female IBS patients have linked increased permeability to altered functional and structural brain connectivity.⁸ Thus, although responses to colorectal distension can be mediated by spinal reflexes and sensory, limbic, and paralimbic regions of the brain,⁹ we asked if neuronal activation was modified by CAMLCK-induced permeability increases. C-Fos immunolabeling, an indicator of neuronal activity, was significantly greater in the paraventricular nucleus of the thalamus, the paraventricular nucleus of the hypothalamus, and the hippocampus but not the medial prefrontal cortex, nucleus accumbens, or amygdala of *CAMLCK^{Tg}*, relative to WT, mice (Figure 2, Supplementary Figure S2). Increased intestinal permeability may therefore increase basal neuronal activity in areas of the brain that regulate responses to visceral pain or stress⁹ but not those associated with conscious visceral sensation.

These results demonstrate that increased intestinal permeability can impact (1) gut microbiome composition,

(2) behavior, (3) visceral pain responses, and (4) neuronal activation within the brain. Critically, these changes are all results, rather than causes, of intestinal barrier loss, as the latter was induced by targeted CAMLCK expression.

The sites of neuronal activation in *CAMLCK^{Tg}* mice support the hypothesis that increased intestinal permeability can activate the hypothalamic-pituitary-adrenal axis.¹⁰ Conversely, hypothalamic-pituitary-adrenal axis activation by exogenous stress can induce intestinal permeability increases.³ Thus, as has been proposed in inflammatory bowel disease and graft-versus-host disease, a self-amplifying cycle may ultimately direct the diverse phenotypes induced by MLCK-dependent, intestinal permeability increases. Further study is needed to define the complex relationships between intestinal permeability, stress, behavioral alterations, visceromotor responses, microbiome composition, and other abnormalities.

These data are the first to assess behavior in a model in which a targeted increase in intestinal tight junction permeability is the only direct perturbation. The results

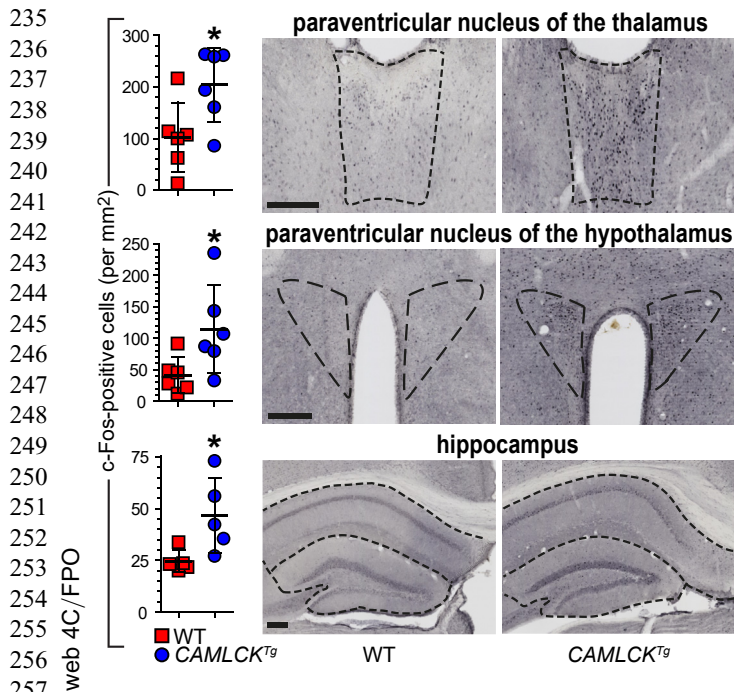


Figure 2. Increased intestinal permeability induces increased c-Fos immunolabeling in selected brain regions. *CAMLCK^{Tg}* (blue circles, n = 5–6) and WT (red squares, n = 5–6) littermates. Representative images of c-Fos-immunolabeled brains from *CAMLCK^{Tg}* and WT mice. Scale bars = 200 μ m. Values are mean \pm SEM. * P < .05, t test.

demonstrate, unequivocally, that modest tight junction permeability increases induced via a physiologically and pathophysiologically relevant mechanism are sufficient to trigger local and systemic microbial, behavioral, and neurosensory changes. This provides a new perspective with which to understand previously hypothesized cause-effect relationships that have been proposed on the basis of correlative data.

References

1. Su L, et al. *Gastroenterology* 2009;136:551–563.
2. Edelblum KL, et al. *Cell Mol Gastroenterol Hepatol* 2017; 4:285–297.
3. Meddings JB, et al. *Gastroenterology* 2000; 119:1019–1028.
4. Yu D, et al. *Proc Natl Acad Sci U S A* 2010;107:8237–8241.
5. Rincel M, et al. *Psychopharmacology (Berl)* 2019; 236:1583–1596.
6. Larauche M, et al. *Neurogastroenterol Motil* 2012;24, 1031–e547.
7. Guerrero-Alba R, et al. *Gut* 2017;66:2121–2131.
8. Witt ST, et al. *Neuroimage Clin* 2019;21:101602.
9. Larauche M, et al. *Neurogastroenterol Motil* 2019;31:e13489.
10. Ait-Belgnaoui A, et al. *Psychoneuroendocrinology* 2012; 37:1885–1895.

Received January 14, 2020. Revised February 26, 2020. Accepted February 27, 2020.

Correspondence

Address correspondence to: Laurent Ferrier, PhD, Nestlé Research, Institute of Health Sciences, Department of Gastro-Intestinal Health, Route du Jorat 57 - Vers-chez-les-Blanc, 1000 Lausanne 26, Switzerland. e-mail: laurent.ferrier@rd.nestle.com; fax: ●●●; or Jerrold R Turner, MD, PhD, Harvard Medical School, Department of Pathology, 77 Avenue Louis Pasteur, NRB 730, Boston, MA 02115; or e-mail: jturner@bwh.harvard.edu; fax: ●●●.

Conflicts of Interest

These authors disclose the following: Jerrold R. Turner is a cofounder of Thelium Therapeutics. Laurent Ferrier is currently an employee of Nestlé Research (Société des Produits Nestlé S.A.). The remaining authors disclose no conflicts.

Funding

This work was supported by an institutional grant from INRA and by National Institutes of Health grants R01DK61931 and R01DK68271 (to Jerrold R. Turner). Muriel Darnaudéry was supported by Bordeaux University, the FFAS (Fond Français Alimentation Santé), and the ANR (Agence Nationale de la Recherche). Marion Rincel was supported by the French ministry of research and education and Labex Brain. Julie Thomas was a recipient of a fellowship from the French Society of Paediatric Research. Orsolya Inczeffi was a recipient of a fellowship from the Nutrition, Chemical Food Safety and Consumer Behaviour Division of INRA.

353 Supplementary Methods

354 Animals

355 *CAMLCK^{Tg}* mice¹⁻⁴ (Tg(Vil-FLAG-CAMLCK)#Jrt) were
 356 maintained as male heterozygotes on C57BL/6J background.
 357 These were mated with wild-type (WT) C57BL/6J female mice
 358 to produce WT and *CAMLCK^{Tg}* littermates. At weaning, female
 359 mice were separated and housed at constant temperature (22
 360 ± 1°C) with a 12-hour light/dark cycle. Food (Teklad 2018;
 361 Envigo, Indianapolis, IN) and water were available ad libitum.
 362 All experiments were performed at 8 weeks of age. Proceed-
 363 ures were approved by the Ethical Committee CEEA-86, under
 364 the number APAFiS#4145.

365 Gut Microbiota Composition Analysis

366 Gut microbiota were analyzed in two cohorts (15 WT
 367 and 16 *CAMLCK^{Tg}*) from 8 different WT dams. At sacrifice,
 368 colonic contents were stored at -80°C. DNA was extracted
 369 using the ZR fecal DNA MiniPrep kit (Zymo Research, Irvine,
 370 CA) and adjusted to 1 ng/μL. Changes in relative abundance
 371 of 24 microbial 16S rRNA gene targets were obtained by
 372 quantitative reverse-transcription polymerase chain reac-
 373 tion (PCR) using an adapted Gut Low-Density Array
 374 platform.⁵⁻⁷ A universal bacterial primer set was included
 375 as the reference gene. quantitative reverse-transcription
 376 PCR was performed in duplicate on a ViiA7 (Applied Bio-
 377 systems, Foster City, CA).

378 Fluorescence data were imported into LinRegPCR to
 379 perform baseline corrections, calculate mean PCR efficiency
 380 per amplicon group, and calculate initial quantities. Among the
 381 24 targeted amplicon groups, 6 were not detected in any fecal
 382 samples and were removed from the analysis (*Bacteroides*
 383 *vulgatus*, *Alistipes* spp, *Parabacteroidetes distasonis*, *Roseburia*
 384 *spp*, *Escherichia coli*, and *Akkermansia muciniphila*). Normal-
 385 ized N₀-values were log₁₀-transformed and processed by
 386 mixOmics (v6.1.1; [https://www.bioconductor.org/packages/
 387 release/bioc/html/mixOmics.html](https://www.bioconductor.org/packages/release/bioc/html/mixOmics.html)) with RStudio (v1.0.44;
 388 RStudio, Boston, MA) to build a partial least-squares
 389 discriminant analysis. This multivariate supervised approach
 390 projects samples (X) onto a low-dimensional space of latent
 391 variables to maximize separation between groups according
 392 (Y = genotype). Leave-one-out cross-validation was used to
 393 select the optimal number of latent variables for partial least-
 394 squares discriminant analysis models.

395 Open Field Test

396 Mice explored a 50 × 50 cm arena (illumination 300 lx)
 397 for 10 minutes. Exploration was automatically assessed
 398 using a video tracking system (Bioseb, Vitrolles, France).
 399 The percentage of distance traveled and time spent and in
 400 the center area (20 × 20 cm) and total distance traveled in
 401 the entire arena were assessed.

402 Colorectal Distension

403 Two 0.08-mm diameter electrodes were implanted in
 404 the abdominal external oblique muscle and a third in the
 405 abdominal skin. On postoperative days 3-6, colorectal
 406 distension (CRD) was performed using a balloon catheter
 407 (Fogarty 4F catheter [Edwards Lifesciences, Irvine, CA], 1.1

408 cm length, tip 3.5 cm from the anus)⁸ in 10-second periods 412
 409 with increasing volumes from 0.02 mL to 0.10 mL, with 5 413
 410 minutes' rest between distensions. Abdominal electromy- 414
 411 ography activity was registered after the amplification 415
 412 (10,000×) and analyzed (Powerlab Chart 5; ADInstruments, 416
 413 Sydney, Australia). Basal electromyographic activity was 417
 414 subtracted from electromyographic activity registered dur- 418
 415 ing distension. Some mice were treated with ML-7 (2 mg/kg 419
 416 intraperitoneal) or naloxone sulfate (2 mg/kg intraperito- 420
 417 neal) 1 hour before CRD. For others, water avoidance stress 421
 418 was induced on a floating platform (3 × 3 cm) in the middle 422
 419 of a water-filled tank (40 × 40 cm) for 1 hour daily over 423
 420 four days. Recovery (30 minutes) preceded CRD. 424
 421 425

426 Gastrointestinal Transit

427 Animals received 70 μL of 100-mg/mL TRITC-70kDa 428
 428 dextran in tap water by gavage and were sacrificed 1 hour 429
 429 later.⁹ The stomach and small and large intestine were cut in 430
 430 11 equal parts. Luminal contents of each segment were 431
 431 centrifuged and fluorescence determined. Transit was calcu- 432
 432 lated as the geometric center of the values for each mouse. 433

434 Ussing Chamber Analysis

435 Jejunal sections were mounted in Ussing chambers 436
 436 (Physiologic Instruments, San Diego, CA) filled with Krebs 437
 437 buffer and continuously oxygenated (95% O₂, 5% CO₂). 438
 438 After 1 hour of equilibration, fluorescein (1 mg/mL) was 439
 439 added in the apical chamber and fluorescence intensity of 440
 440 the basolateral chamber was measured after 1 hour. 441

442 In Vivo Permeability Analysis

443 Mice were fasted for 4 hours before gavage with 150 μL of 444
 444 100-mg/mL FITC-4kDa dextran in tap water. Blood (200 μL) 445
 445 was collected after 4 hours and plasma fluorescence 446
 446 determined. 447

448 C-Fos Analysis

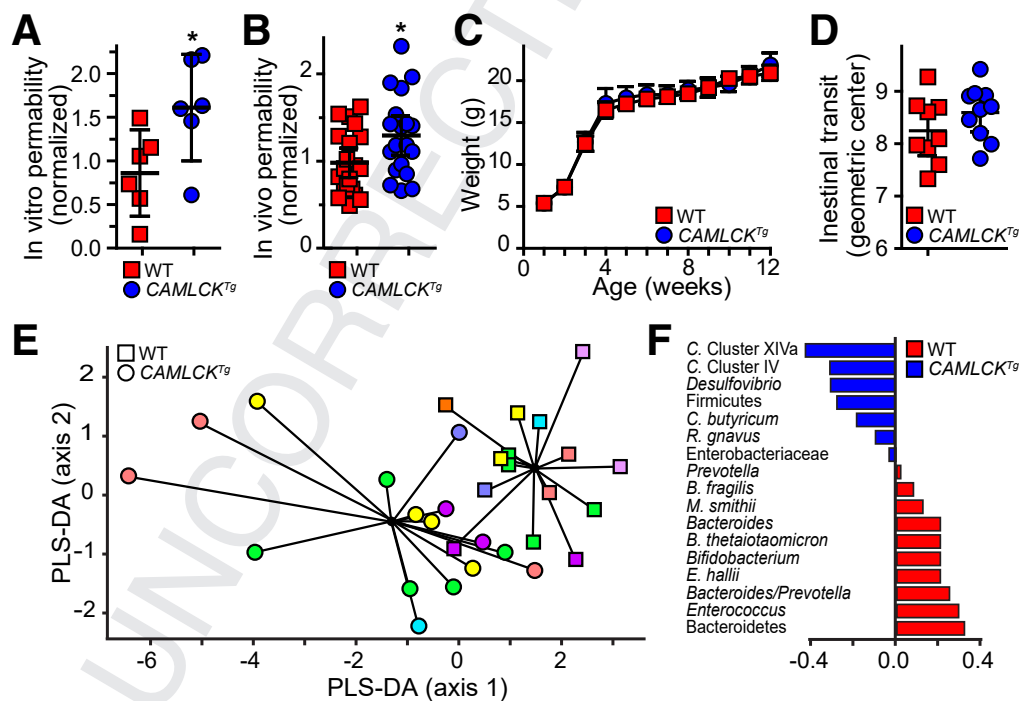
449 Vibratome sections (40 μm) were stained using poly- 450
 450 clonal rabbit anti-c-Fos (Santa Cruz Biotechnology, Dallas, 451
 451 TX) and secondary horseradish peroxidase-conjugated goat 452
 452 anti-rabbit antisera (Jackson ImmunoResearch, West Grove, 453
 453 PA). NDPI images (×20) were obtained (Nanozoomer; 454
 454 Hamamatsu Photonics, Hamamatsu, Japan) and converted 455
 455 into TIFF format using ImageJ (NDPI tools plugin; National 456
 456 Institutes of Health, Bethesda, MD). Regions of interest were 457
 457 manually circumscribed using region-of-interest tools and 458
 458 c-Fos-immunoreactive cells quantified automatically using 459
 459 the particle analysis function (size: 5-20 μm²; circularity: 460
 460 0.5-1). For each animal, 3-6 sections of each brain area 461
 461 were assessed by a blinded observer. 462

463 Statistical Analysis

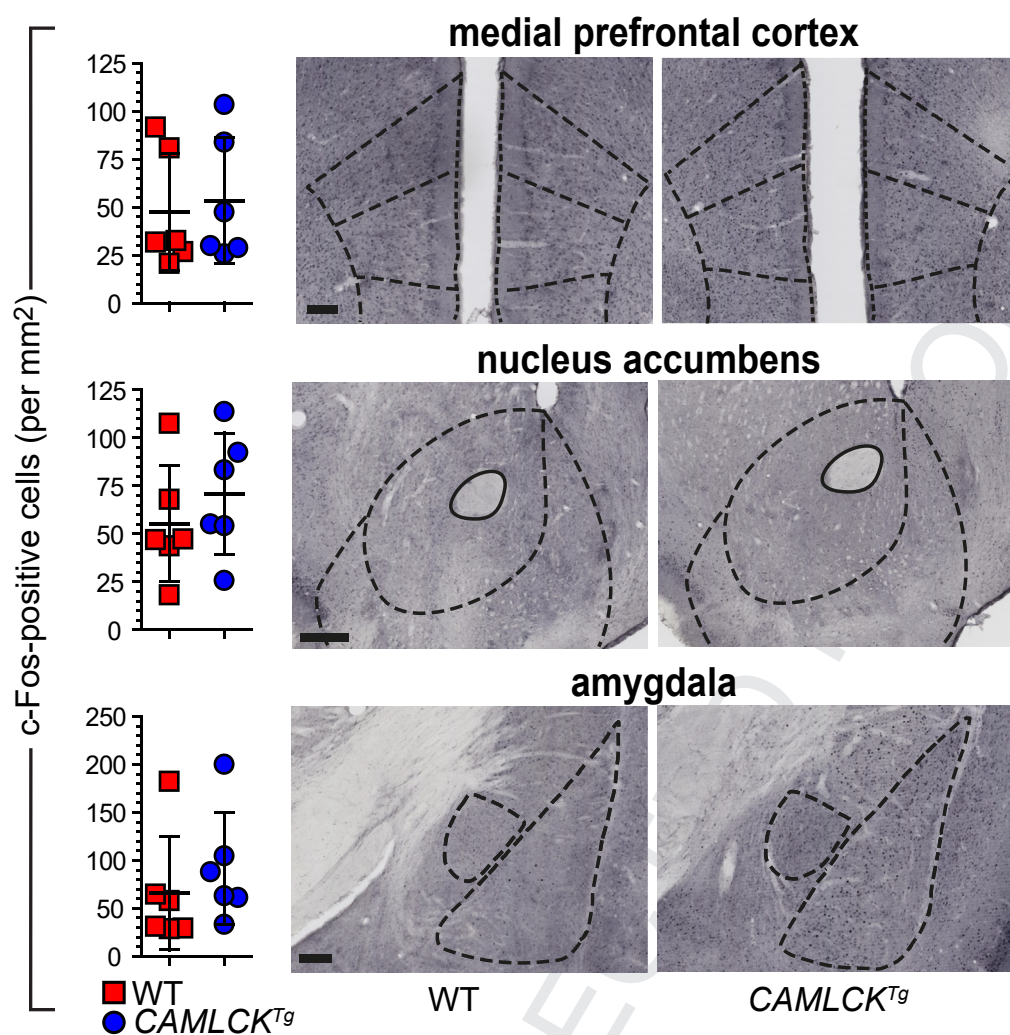
464 Statistical significance was determined by 2-tailed *t* test, 465
 465 2-tailed Mann-Whitney *U* test, or 2-way analysis of variance and 466
 466 set at *P* < .05. For microbial analyses, univariate analysis was 467
 467 realized in parallel to compare each amplicon separately using 468
 468 unpaired *t* test followed by the Benjamini-Hochberg adjust- 469
 469 ment of *P* values for multiple comparisons. 470

471
472
473
474
475
476
477
478
479
480
481
482
483
484
485
486
487
488
489
490
491
492
493
494
495
496
497
498
499
500
501
502
503
504
505
506
507
508
509
510
511
512
513
514
515
516
517
518
519
520
521
522
523
524
525
526
527
528
529**Supplementary References**

1. Su L, et al. *Gastroenterology* 2009;136:551–563.
2. Weber CR, et al. *J Biol Chem* 2010;285:12037–12346.
3. Edelblum KL, et al. *Cell Mol Gastroenterol Hepatol* 2017; 4:285–297.
4. Yu D, et al. *Proc Natl Acad Sci U S A* 2010;107:8237–8241.
5. Bergstrom A, et al. *FEMS Microbiol Lett* 2012;337:38–47.
6. Bergstrom A, et al. *Appl Environ Microbiol* 2014; 80:2889–2900.
7. Riba A, et al. *Gastroenterology* 2017;153:1594–1606.e2.

530
531
532
533
534
535
536
537
538
539
540
541
542
543
544
545
546
547
548
549
550
551
552
553
554
555
556
557
558
559
560
561
562
563
564
565
566
567
568
569
570
571
572
573
574
575
576
577
578
579
580
581
582
583
584
585
586
587
588

Supplementary Figure 1. (A) Transjejunal fluorescein flux was increased in *CAMLCK^{Tg}* (blue circles) relative to wild-type (WT) (red squares) littermates. Values are mean \pm SD. * $P < .05$, Mann-Whitney U test. (B) In vivo analysis using FITC-4kDa dextran demonstrated increased permeability of *CAMLCK^{Tg}* (blue circles, $n = 19$) relative to WT (red squares, $n = 20$) littermates. Values are mean \pm SD. * $P < .05$, t test. (C) Weight gain was similar in WT (red squares, $n = 6$) and *CAMLCK^{Tg}* (blue circles, $n = 6$) littermates. Values are mean \pm SD. (D) Intestinal transit was similar in WT (red squares, $n = 10$) and *CAMLCK^{Tg}* (blue circles, $n = 9$) littermates. Values are mean \pm SD. (E) Partial least-squares discriminant analysis (PLS-DA) score plot based on the relative abundances of 18 microbial taxa in gut contents of *CAMLCK^{Tg}* (circles, $n = 16$) and WT (squares, $n = 15$) born to 8 different dams (each color represents 1 dam). (F) Relative abundances of microbial communities in *CAMLCK^{Tg}* (blue) and WT (red) mice. Diagrams indicate regions analyzed.



Supplemental Figure 2. *CAMLCK^{Tg}* (blue circles, n = 5–6) and wild-type (WT) (red squares, n = 5–6) littermates. Representative images of c-Fos-immunolabeled brains from *CAMLCK^{Tg}* and WT mice. Scale bars = 200 μ m. Values are mean \pm SD. **P* < .05, *t* test.